Unified description of Bessel X waves with cone dispersion and tilted pulses

Miguel A. Porras
Departamento de Física Aplicada, ETSIM, Universidad Politécnica de Madrid, Rios Rosas 21, 28003 Madrid, Spain

Gintaras Valiulis
Department of Quantum Electronics, Vilnius University, Building 3, Sauletekio Avenue 9, Building 3, LT-2040, Vilnius, Lithuania

Paolo Di Trapani
Istituto Nazionale di Fisica della Materia, and Dipartimento di Scienze Chimiche, Fisiche e Matematiche, Università dell'Insubria, Via Valleggio 11, 22100 Como, Italy

(Received 8 February 2003; published 24 July 2003)

We study Bessel X waves with cone dispersion propagating in free space and dispersive media. Their propagation features find simple explanation when viewed as cylindrically symmetric versions of the so-called tilted pulses. All previously reported cases of suppression of normal material group velocity dispersion by using angular dispersion in tilted pulses, pulsed Bessel beams, and Bessel X waves are compared and presented in a unified way. We show that stationary, spatiotemporal localized Bessel X-wave transmission is also possible in the anomalous dispersion regime.

DOI: 10.1103/PhysRevE.68.016613 PACS number(s): 42.65.Tg, 42.65.Re

I. INTRODUCTION

Nondiffracting Bessel beams [1] and their polychromatic versions, namely, X waves [2] and Bessel X waves [3], have been intensively studied after the works by Durnin *et al.* [1]. These beams and pulses are often referred to as conical waves because of the characteristic conical distribution of their elemental plane-wave constituents.

Many degrees of freedom of polychromatic Bessel beams, such as the azimuthal and spectral ones, have been exploited to construct nondiffracting waves with different vorticities and specific temporal characteristics (for a review, see, for example Ref. [4]). The term Bessel X waves [5], for instance, was coined for polychromatic Bessel beams with a narrow spectrum about some optical carrier frequency. Other free parameters, however, have been given less attention. In particular, the cone angle has been generally assumed to take, except for exceptions [6,7], a fixed and the same value θ for all monochromatic Bessel beam constituents. However, cone dispersion, i.e., variation of the cone angle with frequency, is not only unavoidable with most of the Bessel beam generators (axicons, Fourier lenses, circular diffraction gratings, etc.), but also desirable for some applications, as demonstrated in Ref. [7] for the suppression of temporal broadening of pulses due to material dispersion. In nonlinear optics, on the other hand, femtosecond Bessel X waves with cone dispersion have been demonstrated to be spontaneously generated in the process of second-harmonic generation in normally dispersive nonlinear media [8–10]. Angular dispersion appears here as the natural mechanism of phase matching of the different monochromatic Bessel beam constituents [9–12].

The main purpose of this work is to provide a simple and useful description of the propagation features of Bessel X waves (BXW) with dispersion in the cone angle. The propagation medium may be free space or a dispersive medium indifferently, but the latter case is more interesting because of the phenomena arising from the interplay of material and angular dispersion. Dispersive BXWs (in the sense of cone and/or the material dispersion) constitute a family of generalized nondiffracting waves, in the sense that the transversal *energy density* distribution remains invariant during propagation. Unlike nondispersive BXWs in free space, the effects of cone and/or material dispersion make the *intensity* distribution to change in space and time in a rather complicated way.

At this point our task is greatly simplified with the help of tilted pulses (TPs) [13], which are shown to be the two-dimensional versions of the three-dimensional, axisymmetric BXWs. The TPs, or plane pulses with angular dispersion, are produced by angularly dispersive optical elements, such as diffraction gratings or prisms, that divert differently each monochromatic component of the pulse. They have found broad application in nonlinear femtosecond optics for controlling group velocity dispersion and group velocity mismatch for temporal and spatiotemporal soliton formation in $\chi^{(2)}$ media [14,15]. The primary effects of angular dispersion are the tilting of the pulse front with respect to the phase front [16–18], and the negative group velocity dispersion [13,19,20], an effect that was earlier used as a linear mechanism of pulse compression [17,21].

The first part of this paper (Sec. II) is then devoted to recall the essential features of TPs, and to describe some unknown aspects of their spatiotemporal structure, which are essential for understanding the dispersive BXWs. Next, we characterize the spatiotemporal behavior of BXWs with cone dispersion $\theta(\omega)$ in the simpler terms of the associated TP with the same angular dispersion $\theta(\omega)$ (Sec. III). The relevant propagation features of TPs and BXWs find unified explanation in terms of three vectors, $\boldsymbol{k}_0$, $\boldsymbol{k}_0'$ and $\boldsymbol{k}_0''$, having different directions, that generalize the usual scalar quantities k_0, k_0', and k_0'' to include the effects of angular dispersion together with those of material dispersion (if any). Within this unified theory, a third kind of wave, the so-called pulsed Bessel beam (PBB) [22,23], appears as a particular, degen-

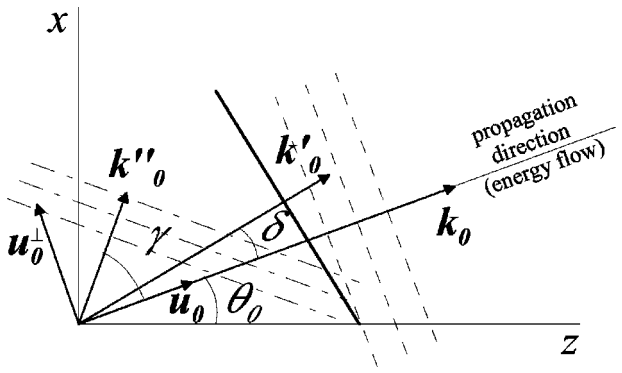

FIG. 1. Schematic drawing of the TP properties. Pulse front—solid line; wave fronts—dashed lines; and planes of constant width: dot-dashed lines.

erated member of the dispersive BXW family. Also, previously described and seemingly disconnected techniques for suppression of group velocity dispersion (GVD) in normally dispersive media with TPs [24], PBBs [22,25], and BXWs [5–7] can be understood from a common point of view (Sec. IV). We conclude this paper (Sec. V) by showing that BXWs can also propagate without GVD temporal spreading in media with anomalous dispersion.

II. SPATIOTEMPORAL STRUCTURE OF TILTED PULSES

The propagation features of TPs can be easily described from their representation as a superposition of monochromatic plane waves propagating in different directions. Referring to the two-dimensional geometry of Fig. 1, a TP can be expressed as

$$E(\boldsymbol{r},t)=\frac{1}{\pi}\int_0^\infty d\omega\hat{f}(\omega)\exp[i\boldsymbol{k}(\omega)\cdot\boldsymbol{r}]\exp(-i\omega t), \quad (1)$$

where $\hat{f}(\omega)$ is some narrow spectral amplitude function about some angular frequency ω_0, $\boldsymbol{r}\equiv(x,z)$, $\boldsymbol{k}(\omega)\equiv(k_x(\omega),k_z(\omega))=k(\omega)\boldsymbol{u}(\omega)$ is the wave vector of each monochromatic plane-wave component of frequency ω. The modulus $k(\omega)$ of the wave vector is the propagation constant; in free space $k(\omega)=\omega/c$ and in a dispersive medium $k(\omega)=n(\omega)\omega/c$, where $n(\omega)$ is the refraction index. The unit vector $\boldsymbol{u}(\omega)=\sin\theta(\omega)\boldsymbol{u}_x+\cos\theta(\omega)\boldsymbol{u}_z$ forms an angle $\theta(\omega)$ with the z axis, and determines the propagation direction of each monochromatic plane wave. For simplicity, prime signs throughout this paper will mean differentiation with respect to angular frequency ω, and subscripts 0 evaluation at the carrier frequency ω_0. For instance, $\theta_0'\equiv d\theta(\omega)/d\omega|_{\omega_0}$.

Writing the spectrum phase $\varphi_\omega(\boldsymbol{r})=\boldsymbol{k}(\omega)\cdot\boldsymbol{r}$ as the Taylor power series $\varphi_\omega(\boldsymbol{r})=\varphi_0(\boldsymbol{r})+\varphi_0'(\boldsymbol{r})(\omega-\omega_0)+\varphi_0''(\boldsymbol{r})(\omega-\omega_0)^2/2+\cdots$, where

$$\varphi_0(\boldsymbol{r})=\boldsymbol{k}_0\cdot\boldsymbol{r},$$

$$\varphi_0'(\boldsymbol{r})=\boldsymbol{k}_0'\cdot\boldsymbol{r},$$

$$\varphi_0''(\boldsymbol{r})=\boldsymbol{k}_0''\cdot\boldsymbol{r},$$

$$\vdots \quad (2)$$

we can conveniently express the TPs Eq. (1), as enveloped carrier oscillations of the form

$$E(\boldsymbol{r},t)=A(\boldsymbol{r},t)\exp\{-i[\omega_0 t-\varphi_0(\boldsymbol{r})]\}, \quad (3)$$

where the envelope is given by

$$A(\boldsymbol{r},t)=\frac{1}{\pi}\int_0^\infty d\omega\hat{f}(\omega)\exp\left[\frac{i}{2}\varphi_0''(\boldsymbol{r})(\omega-\omega_0)^2+\cdots\right]\times\exp\{-i(\omega-\omega_0)[t-\varphi_0'(\boldsymbol{r})]\}. \quad (4)$$

The field expressed by Eqs. (3) and (4) is a three-dimensional wave packet whose spatiotemporal structure is characterized, up to second order in dispersion [23,26], by (1) its wave fronts $\varphi_0(\boldsymbol{r})=\text{const}$, or surfaces of constant phase of the carrier oscillations, that propagate at the phase velocity $v_p=\omega_0/|\text{grad}\varphi_0(\boldsymbol{r})|$; (2) its pulse front $\varphi_0'(\boldsymbol{r})=t$, or geometrical locus of points where the pulse peak arrives at the same time t, a surface that propagates at the group velocity $v_g=1/|\text{grad}\varphi_0'(\boldsymbol{r})|$; and (3) the surfaces of equal spectrum chirp $\varphi_0''(\boldsymbol{r})=\text{const}$, or geometrical locus of points of equal pulse duration [23].

In the specific case of the TPs, the wave front equation is given, from Eqs. (2), by $\boldsymbol{k}_0\cdot\boldsymbol{r}=\text{const}$. Wave fronts (dashed lines of Fig. 1) are then planes perpendicular to the carrier wave vector

$$\boldsymbol{k}_0=k_0\boldsymbol{u}_0, \quad (5)$$

where $\boldsymbol{u}_0=\boldsymbol{u}_x\sin\theta_0+\boldsymbol{u}_z\cos\theta_0$ (see Fig. 1), that propagates at the phase velocity

$$v_p=\frac{\omega_0}{|\boldsymbol{k}_0|}=\frac{\omega_0}{k_0}. \quad (6)$$

The pulse front $t=\boldsymbol{k}_0'\cdot\boldsymbol{r}$ is also a plane (solid line of Fig. 1), but it is perpendicular to the vector

$$\boldsymbol{k}_0'=k_0'\boldsymbol{u}_0+k_0\theta_0'\boldsymbol{u}_0^\perp, \quad (7)$$

where $\boldsymbol{u}_0^\perp=\boldsymbol{u}_x\cos\theta_0-\boldsymbol{u}_z\sin\theta_0$ is a unit vector perpendicular to $\boldsymbol{u}_0$ (see Fig. 1). The component of $\boldsymbol{k}_0'$ in the direction of $\boldsymbol{u}_0^\perp$ originates from angular dispersion ($\theta_0'\neq0$), and causes the pulse front to be tilted with respect to the wave fronts (Fig. 1), as is well-known, a certain angle δ (tilt angle), given by

$$\tan\delta=\frac{k_0}{k_0'}\theta_0'. \quad (8)$$

The pulse front propagates at the group velocity

$$v_g=\frac{1}{|\boldsymbol{k}_0'|}=\frac{1}{\sqrt{k_0'^2+k_0^2\theta_0'^2}}, \quad (9)$$

slower than the group velocity of a plane pulse in the same medium.

The most known property of TPs is the GVD that originates from angular dispersion [13,19,20]. Spectrum chirp is constant on the planes $\boldsymbol{k}_0''\cdot\boldsymbol{r}=\text{const}$ (dot-dashed lines of Fig. 1), perpendicular to the GVD vector,

$$\boldsymbol{k}_0''=(k_0''-k_0\theta_0'^2)\boldsymbol{u}_0+(2k_0'\theta_0'+k_0\theta_0'')\boldsymbol{u}_0^{\perp}, \tag{10}$$

which forms an angle γ with the direction of propagation of wave fronts, given by

$$\tan\gamma=\frac{2k_0'\theta_0'+k_0\theta_0''}{k_0''-k_0\theta_0'^2}. \tag{11}$$

On the planes $\boldsymbol{k}_0''\cdot\boldsymbol{r}=\text{const}$, pulse duration does not change (if higher-order dispersion effects are neglected). Along the direction of the GVD vector $\boldsymbol{k}_0''$, however, pulse duration changes at a maximum rate, with a GVD parameter (spectrum chirp per unit length) given by

$$|\boldsymbol{k}_0''|=\sqrt{(k_0''-k_0\theta_0'^2)^2+(2k_0'\theta_0'+k_0\theta_0'')^2}. \tag{12}$$

All previous features are summarized in Fig. 1, in which the three vectors $\boldsymbol{k}_0$, $\boldsymbol{k}_0'$, and $\boldsymbol{k}_0''$, and the associated wave fronts, pulse front, and the planes of constant pulse duration are sketched. Higher-order dispersion vectors $\boldsymbol{k}_0^{(n)}$ and the corresponding planes can be obviously introduced for a more accurate description of TPs.

By definition, the phase and group velocities of Eqs. (6) and (9) are the velocities of propagation of the wave fronts and pulse front, respectively, perpendicular to themselves [26]. Similarly, $|\boldsymbol{k}_0''|$ is the GVD parameter along a direction perpendicular to the planes of constant duration. For TPs (and BXW below), however, these directions are not the only ones of interest. Along any other spatial direction, the temporal characteristics of the TP are determined by the projections of the vectors $\boldsymbol{k}_0$, $\boldsymbol{k}_0'$, and $\boldsymbol{k}_0''$ over that direction. Let us consider, for example, the TP features over the direction of propagation of the wave fronts ($\boldsymbol{k}_0$). Note that, if the medium is isotropic, this direction coincides with the direction of energy flow [26]. We can therefore identify it with the actual propagation direction of the TP. Wave fronts and pulse front appear to advance along the energy flow direction at the effective phase and group velocities

$$v_{p,u_0}=\frac{\omega_0}{\boldsymbol{k}_0\cdot\boldsymbol{u}_0}=\frac{\omega_0}{k_0}, \tag{13}$$

$$v_{g,u_0}=\frac{1}{\boldsymbol{k}_0'\cdot\boldsymbol{u}_0}=\frac{1}{k_0'}, \tag{14}$$

respectively, and pulse duration changes with an effective GVD

$$k_{0,u_0}''=\boldsymbol{k}_0''\cdot\boldsymbol{u}_0=k_0''-k_0\theta_0'^2=k_0''-\frac{k_0'^2}{k_0}\tan^2\delta. \tag{15}$$

Equations (13)–(15) for the effective phase, and group velocities and GVD, together with Eq. (8), are the well-known properties of TPs in isotropic media. The net effect of angular dispersion is then to create a pulse tilt [16–18] and to change the GVD from its value k_0'' for a plane pulse [13,19,20]. In particular, the tilt angle in vacuum is given by $\tan\delta=\omega_0\theta_0'$, the phase and group velocities equal to c, and the GVD induced by angular dispersion is $-\omega_0\theta_0'^2/c$, always negative [19].

Note that all the properties of TPs are obviously independent of θ_0, since the orientation of the axes x,z is arbitrary. Indeed, the natural choice for the description of TPs is $\theta_0=0°$. For BXWs in Sec. III, however, the energy flow direction ($\boldsymbol{k}_0$) forms, in general, a certain angle $\theta_0\neq 0°$ with another privileged direction, the revolution axis, which will be taken to be the z axis.

From Fig. 1, pulse broadening along the propagation direction ($\boldsymbol{k}_0$) of a TP can be understood from the fact that different points along this direction belong to different planes of constant duration (dash-dotted lines). To understand Bessel X waves, we also note that, for the same reason, pulse duration is not constant over the pulse front and, in general, along any other direction. The corresponding GVD can be calculated as the scalar product $\boldsymbol{k}_0''\cdot\boldsymbol{u}$, where is $\boldsymbol{u}$ is a unit vector along the specified direction.

As an example, Figs. 2(a)–2(c) show gray-scale plots of the intensity $|E(\boldsymbol{r},t)|^2$ of a free-space TP with angular dispersion curve $\theta(\omega)=0.175+0.02(\omega-\omega_0)+0.005(\omega-\omega_0)^2$, $\omega_0=3.14$ fs^{-1} and spectrum $\hat{f}(\omega)=\exp[-\Delta t^2(\omega-\omega_0)^2/4]$, $\Delta t=2$ fs, at increasing times (a) $t=0$, (b) $t=143$, and (c) $t=428$ fs [they are chosen, for comparison with BXWs in the following section, so that the pulse front $t=\boldsymbol{k}_0'\cdot\boldsymbol{r}$ intersects the axial points $\boldsymbol{r}=(0,0),(0,z_D),(0,3z_D)$, $z_D\equiv\Delta t^2/2|k_{0,z}''|=0.044$ mm]. Wave fronts (which cannot be seen), and hence energy, propagate at $\theta_0=10°$ with respect to the z axis [along vector $\boldsymbol{k}_0$ of Fig. 2(a)], while the pulse front is tilted, from Eq. (8), $\delta=3.6°$ [vector $\boldsymbol{k}_0'$ of Fig. 2(a)] and the GVD vector points, from Eq. (11), at an angle $\gamma=-89°$ with respect to the wave front propagation direction. The pulse broadens over the pulse front and along the z direction because of the nonvanishing projection of $\boldsymbol{k}_0''$ over these directions.

In the first row of Fig. 3, we show the more usual intensity–local-time representation of the same TP as in Fig. 2, that is, the TP temporal form as it passes through the planes (a) $z=0$, (b) $z=z_D$, and (c) $z=3z_D$, taking the time of arrival, $t=k_{0,z}'z$, at each plane as the origin of time. In comparison with Figs. 2(a)–2(c), the only one differences are that Figs. 3(a)–3(c) are specularly reversed with respect to the vertical axis $t-k_{0,z}'z=0$, and the scaling of angles is lost.

III. BESSEL X WAVES WITH CONE DISPERSION

As is well known, Bessel beams result from the superposition of monochromatic plane waves whose wave vectors are evenly distributed over the surface of a cone of a certain half-apex angle θ [1] and BXWs from the superposition of Bessel beams of different frequencies about a central one ω_0.

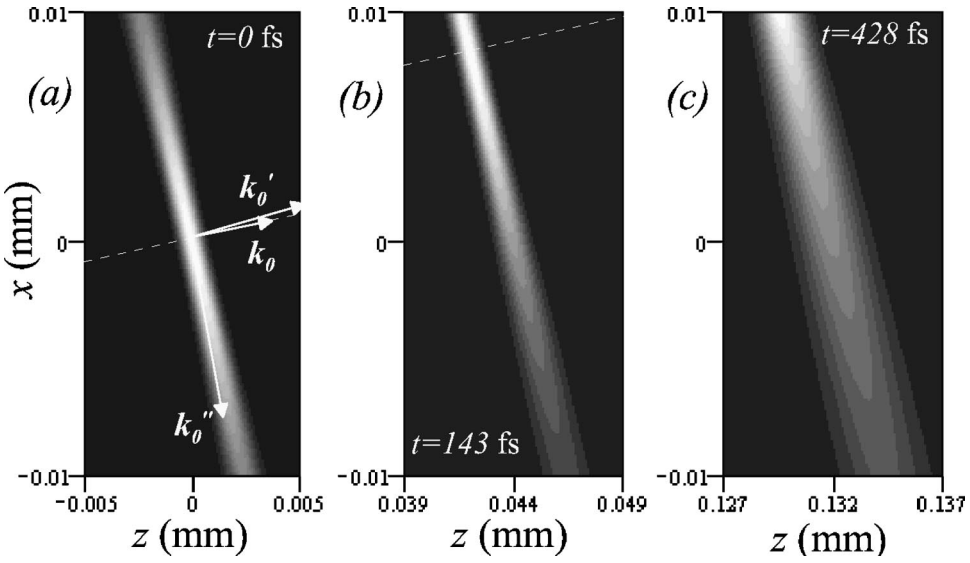

FIG. 2. Gray scale plots of the intensity $|E(\boldsymbol{r},t)|^2$ of TP of Eq. (1) propagating in free space with angular dispersion curve $\theta(\omega)=0.175+0.02(\omega-\omega_0)+0.005(\omega-\omega_0)^2$. The amplitude spectrum is $\hat{f}(\omega)=\exp[-\Delta t^2(\omega-\omega_0)^2/4]$, corresponding to a Gaussian pulse of carrier frequency $\omega_0=3.14\ \mathrm{fs}^{-1}$ and Gaussian half duration $\Delta t=2$ fs. The propagation times are (a) $t=0$ fs, (b) $t=143$ fs, and (c) $t=428$ fs.

Ideally, the different monochromatic Bessel beams have the same cone angle θ, but in practice, all Bessel beam generators, such as Fourier lenses, axicons, diffraction gratings, or holograms, produce Bessel beams with different cone angles for different frequencies. Thus BXWs generated by these linear means will present dispersion in the cone angle, a property that has been shown to be advantageous for some applications such as GVD suppression in dispersive materials [6,7,22,25] (see also Sec. IV). In nonlinear optics, angular dispersion in the BXWs spontaneously generated in the pro-

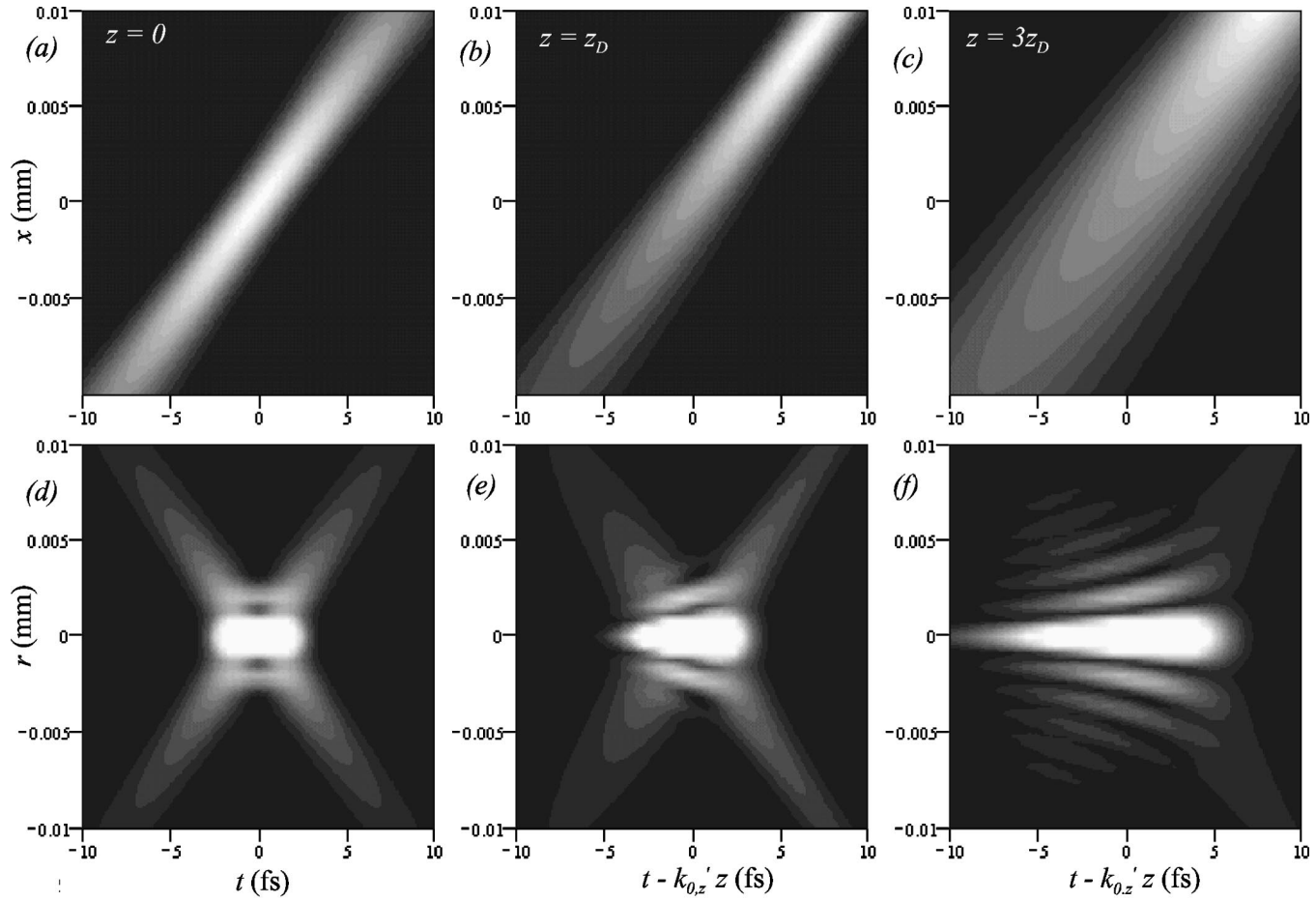

FIG. 3. First row: Gray scale plots of the time variation of the intensity $|E(\boldsymbol{r},t)|^2$ of the TP of Fig. 2 at the planes (a) $z=0$, (b) $z=z_D$, and (c) $z=3z_D$, where $z_D=\Delta t^2/2|k''_{0,z}|=0.044$ mm is the dispersion length along the z direction. Second row: Gray scale plots of the intensity $|E(\boldsymbol{r},t)|^2$ of the BXW of Eq. (17), or revolution symmetry version of the TP of the first row.

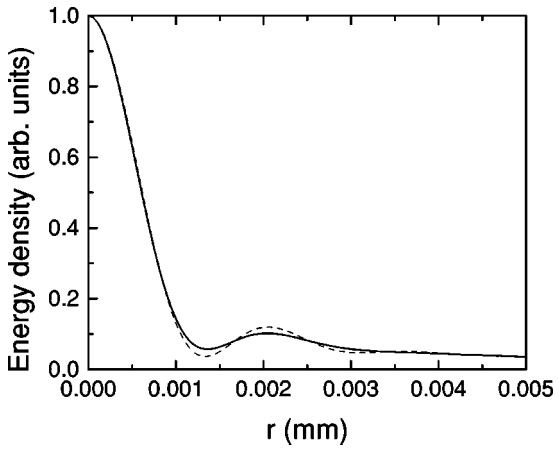

FIG. 4. Transversal energy density distributions $\mathcal{E}(r)$ of the free-space BXWs with cone dispersion curve $\theta(\omega)=0.175+0.02(\omega-\omega_0)+0.005(\omega-\omega_0)^2$ (solid curve) and without angular dispersion, $\theta(\omega)=0.0175$ (dashed curve). The amplitude spectrum is $\hat{f}(\omega)=\exp[-\Delta t^2(\omega-\omega_0)^2/4]$ is both cases, with $\omega_0=3.14$ fs^{-1} and $\Delta t=2$ fs.

cess of second-harmonic generation is essential to achieve phase matching of the different monochromatic components [9]. Despite their ubiquity, and except for some particular GVD-free BXWs [6,22], the propagation features of BXWs with general cone dispersion in dispersive media have not been studied so far. In this section, we show that the relevant propagation features of BXWs with cone dispersion in dispersive media can be easily understood from those of TPs.

Dispersive BXWs can be, in fact, considered as cylindrically symmetric TPs: If we rotate a TP [Eq. (1)] by an arbitrary azimuthal angle ϕ with respect to the z axis ($x\rightarrow x\cos\phi - y\sin\phi$), and integrate over all azimuthal angles ϕ in the range $[0,2\pi]$, we obtain

$$E(x,y,z,t)=\frac{1}{2\pi}\int_0^{2\pi}d\phi\frac{1}{\pi}\int_0^{\infty}d\omega\hat{f}(\omega)\times\exp[ik(\omega)\sin\theta(\omega)r\cos(\phi+\alpha)]\times\exp[ik(\omega)\cos\theta(\omega)z]\exp(-i\omega t), \quad (16)$$

where we have further written $x=r\cos\alpha$, $y=r\sin\alpha$. Integration in ϕ yields

$$E(r,z,t)=\frac{1}{\pi}\int_0^{\infty}d\omega\hat{f}(\omega)J_0[k(\omega)\sin\theta(\omega)r]\times\exp[ik(\omega)\cos\theta(\omega)z]\exp(-i\omega t), \quad (17)$$

with $r=\sqrt{x^2+y^2}$, which is the expression of a BXW with cone dispersion $\theta(\omega)$.

Dispersive BXWs can be still said to be nondiffracting in the sense that the transversal energy density distribution $\mathcal{E}(r)=\int_{-\infty}^{\infty}dt|E(r,z,t)|^2$, or from Parseval's theorem and Eq. (17),

$$\mathcal{E}(r)=\frac{2}{\pi}\int_0^{\infty}d\omega|\hat{f}(\omega)|^2J_0^2[k(\omega)\sin\theta(\omega)], \quad (18)$$

does not depend on propagation coordinate z. Figure 4 shows a typical transversal energy density $\mathcal{E}(r)$ distribution of a free-space BXW with angular dispersion in comparison with that for the same BXW but without angular dispersion.

The field amplitude $E(r,z,t)$ and intensity $|E(r,z,t)|^2$, however, experience changes because of material and angular dispersion. Comparison of Eqs. (1) and (17) shows that the on-axis pulse temporal form of the BXW ($r=0$) is the same as that of the TP ($x=0$), i.e.,

$$E(r=0,z,t)=\frac{1}{\pi}\int_0^{\infty}d\omega\hat{f}(\omega)\exp[ik(\omega)\cos\theta(\omega)z]\times\exp(-i\omega t). \quad (19)$$

In particular, the effective phase velocity, group velocity, and the GVD of the BXW are those of the TP along the z direction, $v_{p,z}=\omega_0/(\boldsymbol{k}_0\cdot\boldsymbol{u}_z)$, $v_{g,z}=1/(\boldsymbol{k}_0'\cdot\boldsymbol{u}_z)$, and $\boldsymbol{k}_{0,z}''=\boldsymbol{k}_0''\cdot\boldsymbol{u}_z$, that is,

$$v_{p,z}=\frac{\omega_0}{k_0\cos\theta_0}, \quad (20)$$

$$v_{g,z}=\frac{1}{k_0'\cos\theta_0-k_0\theta_0'\sin\theta_0}, \quad (21)$$

$$k_{0,z}''=(k_0''-k_0\theta_0'^2)\cos\theta_0-(2k_0'\theta_0'+k_0\theta_0'')\sin\theta_0, \quad (22)$$

or, as functions of the cone angle θ_0, the tilt angle δ, and the GVD angle γ,

$$v_{p,z}=\frac{\omega_0}{k_0\cos\theta_0}, \quad (23)$$

$$v_{g,z}=\frac{\cos\delta}{k_0'\cos(\theta_0+\delta)}, \quad (24)$$

$$k_{0,z}''=\left(k_0''-\frac{k_0'^2}{k_0}\tan^2\delta\right)\frac{\cos(\theta_0+\gamma)}{\cos\gamma}. \quad (25)$$

We then see that the effective phase velocity along the z direction is always equal or larger than that of a plane pulse in the same medium (in particular, luminal or superluminal in vacuum), but contrary to nondispersive BXWs, the group velocity can be smaller, equal or larger than the group velocity of a plane pulse (hence subluminal, luminal or superluminal in vacuum). It is also important to note from Eq. (25) that, unlike TPs, GVD in BXWs induced by cone dispersion can be positive (normal) in vacuum. This situation takes place for angular dispersion such that $\cos(\theta_0+\gamma)<0$, that is, when the vector $\boldsymbol{k}_0''$ has a negative projection over the propagation direction z (see also Sec. V).

If, for instance, we choose the spectral amplitude $\hat{f}(\omega)\propto\exp[-\Delta t^2(\omega-\omega_0)^2/4]$, the initial Gaussian pulse $E(r=0,z=0,t)=\exp[-t^2/\Delta t^2]\exp(-i\omega_0 t)$ transforms into the broadened and chirped Gaussian pulse

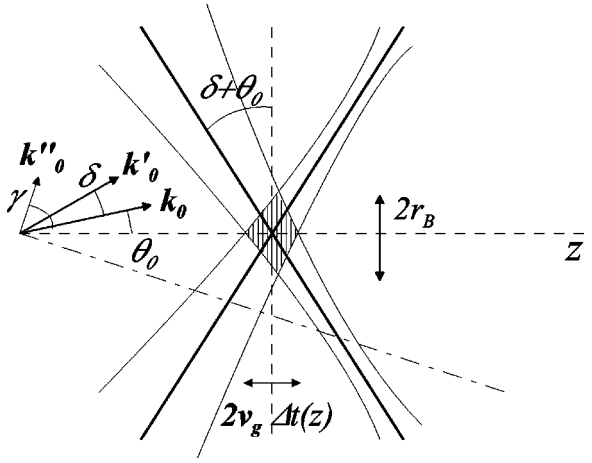

FIG. 5. Understanding the features of BXWs with cone dispersion from those of TPs.

$$E(r=0,z,t)=\left[\frac{1+iC(z)}{\Delta t^2(z)}\right]^{1/2} \times\exp\left[-(t-z/v_{g,z})^2\frac{1+iC(z)}{\Delta t^2(z)}\right] \times\exp(-i\omega_0 t+ik_{z,0}z), \tag{26}$$

where pulse duration and chirp change according to the well-known rules [27]

$$\Delta t(z)=\Delta t\sqrt{1+z^2/z_D^2}, \tag{27}$$

$$C(z)=\mathrm{sgn}(k''_{0,z})z/z_D, \tag{28}$$

and where $z_D=\Delta t^2/2|k''_{0,z}|$ is the effective dispersion length in the z direction. Pulse chirp at propagation distance z makes the instantaneous frequency of the carrier oscillations to change linearly with time as

$$\omega(z,t)=\omega_0+2\frac{C(z)}{\Delta t^2(z)}\left(t-\frac{z}{v_{g,z}}\right). \tag{29}$$

To understand the off-axis properties of dispersive BXWs, we show in Figs. 3(d)–3(f) the cylindrically symmetric BXW version of the TP of Figs. 3(a)–3(c). As in the case of no cone dispersion and free-space propagation described in Ref. [5], dispersive BXWs present some of the characteristic transversal modulations of monochromatic Bessel beams, modulations that cease at some radial distance, from which the pulse behavior resembles that of an X wave. The characteristics of these two regions can be inferred from those of the associated TP. The inclination α of the X tails of the BXW is that of the pulse front of the TP, that is,

$$\alpha=\theta_0+\delta \tag{30}$$

with respect the radial direction (see Fig. 5). Contrary to the nondispersive case, the tails become asymmetric upon propagation [Figs. 3(e) and 3(f)] due to pulse broadening along the pulse front of the TP. In the dashed region of Fig. 5, the carrier oscillations of all TPs with different azimuthal angles interfere, forming, as in the monochromatic case, the characteristic transversal Bessel pattern. If the axial half length of the BXW is $v_{g,z}\Delta t(z)$ (see Fig. 5), the radius of the region of Bessel behavior can be estimated to be

$$r_B(z)\simeq\frac{v_{g,z}\Delta t(z)}{\tan(\theta_0+\delta)}. \tag{31}$$

Contrary to the nondispersive case, the radius of Bessel behavior depends not only on the cone angle θ_0 but also on the tilt angle δ, and increases with propagation distance due to on-axis pulse broadening, as seen in Figs. 3(e) and 3(f). Another significant difference (second row of Fig. 3) is the time-varying period of the Bessel modulations, an effect that originates from pulse chirp. If the size of the Bessel transversal pattern of a monochromatic Bessel beam of frequency ω_0, measured as the first zero of the Bessel function, is $\Delta r_B\simeq 2.4/k_0\sin\theta_0$, for the time-varying frequency of Eq. (29), we should accordingly have

$$\Delta r_B(z,t)\simeq\frac{2.4}{k(\omega(z,t))\sin\theta(\omega(z,t))}, \tag{32}$$

an expression that accurately measures the time-varying spot size of the transversal Bessel profile in all the cases studied. At large propagation distances [Fig. 3(f)], pulse duration $\Delta t(z)$ and chirp $C(z)$ become proportional to propagation distance z; hence $r_B\to\infty$ and $\Delta r_B\to 2.4/k_0\sin\theta_0$, that is, the BXW approaches a monochromatic Bessel beam of frequency ω_0.

In conclusion, we see that the knowledge of the angles θ_0, δ, and γ of the vectors $\boldsymbol{k}_0$, $\boldsymbol{k}'_0$, and $\boldsymbol{k}''_0$ of a TP with angular dispersion curve $\theta(\omega)$ allows us to predict the relevant spatiotemporal features, and their changes upon propagation, of the BXW with the same cone dispersion curve.

A degenerated case: Pulsed Bessel beams

As an example of interest, we consider the TP [Eq. (1)] and the associated BXW [Eq. (17)] with angular and cone dispersion curves $\theta(\omega)=\sin^{-1}[K/k(\omega)]$, $K=$const, produced by a diffraction grating of period $d=2\pi/K$, and a circular diffraction grating [28] of the same period, respectively, at normal incidence. The curve $\theta(\omega)$ and Eqs. (8) and (11) yield the angles $\theta_0=\sin^{-1}(K/k_0)$, $\delta=-\theta_0$, and $\gamma=-\theta_0$. The wave fronts of the TP then travel at the angle θ_0 with respect to the z axis, whereas the pulse front and planes of constant duration are both perpendicular to the z axis, as illustrated in the inset of Fig. 6. As a consequence, pulse duration grows with increasing values of z only and, in particular, is constant over the pulse front. In Fig. 6, these features are shown in a particular case of free-space propagation, in which case pulse broadening originates from angular dispersion solely. The corresponding BXW, referred to in this case as the pulsed Bessel beam [23,25], is shown in the second row of Fig. 6 at several propagation distances. From the values of θ_0, δ, and γ of the TP, and Eqs. (20) and (21), the

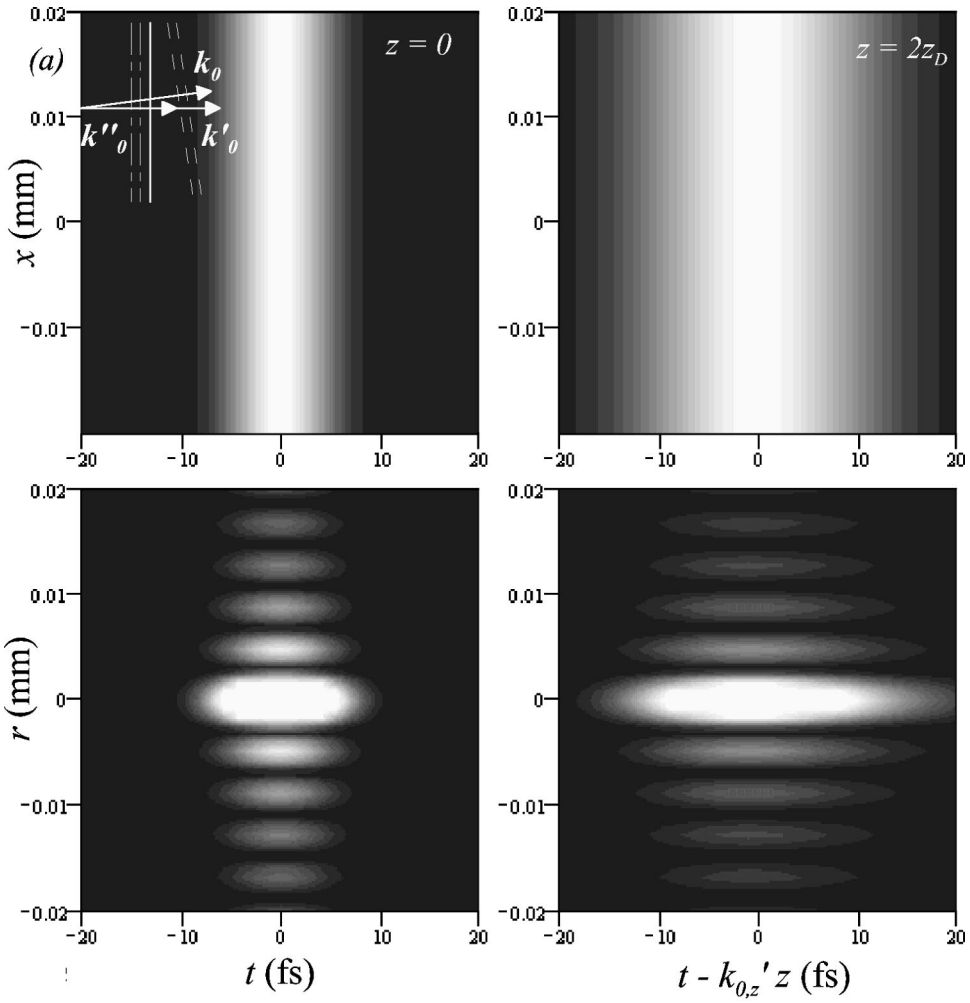

FIG. 6. Inset: schematic drawing of the vectors $\boldsymbol{k}_0$, $\boldsymbol{k}_0'$, and $\boldsymbol{k}_0''$ determining the propagation direction of the wave fronts, pulse front, and planes of constant duration of a TP from a diffraction grating. First row: Gray scale plots of the time variation of the intensity $|E(\boldsymbol{r},t)|^2$ of the free-space TP with diffraction grating angular dispersion curve $\theta(\omega) = \sin^{-1}[Kc/\omega]$, $K = 800\ \mathrm{mm}^{-1}$, and amplitude spectrum $\hat{f}(\omega) \propto \exp[-\Delta t^2(\omega-\omega_0)^2/4]$, $\omega_0 = 1.884\ \mathrm{fs}^{-1}$ ($\lambda_0 = 1\ \mu\mathrm{m}$), $\Delta t = 6.66$ fs. The propagation distances are $z=0$ and $z=z_D$, where $z_D = \Delta t^2/2|k''_{0,z}| = 0.754$ mm. Second row: the same as in the first row, but for the corresponding BXW, or single-tailed PBB.

on-axis phase and group velocities result to $v_{p,z} = \omega_0/k_0 \cos\theta_0$ and $v_{g,z} = \cos\theta_0/k_0'$, which in free space are superluminal and subluminal, respectively. The axial GVD parameter is, from Eq. (22),

$$k''_{0,z} = \frac{1}{\cos\theta_0}\left(k''_0 - \frac{k_0'^2}{k_0}\tan^2\theta_0\right), \tag{33}$$

always negative in free space. Equations (30)–(32) lead, as expected, to $\theta_0 + \delta = 0$ for the inclination of the X tails with respect to the radial direction (so that they degenerate into a single radial one) to $r_B = \infty$ for the radius of the region of the Bessel behavior and to $\Delta r_B = 2.4/K$, independent of time, for the spot size of the radial Bessel profile.

IV. GVD SUPPRESSION IN NORMALLY DISPERSIVE MEDIA WITH TILTED PULSES, PULSED BESSEL BEAMS, AND BESSEL X WAVES

From a number of previous works [5–7,22,24,25], it is a well-established fact that anomalous GVD induced by angular dispersion can compensate for normal GVD of a dispersive material, resulting in the formation of GVD-free TP [24], BXW [5–7], or PBB [22,25] propagating in the dispersive medium. Despite their fundamental similarity, there are significant differences (and possibly misunderstandings) on how compensation is achieved in these three cases. Similarities and differences can be put into evidence from the present unified approach.

A. GVD-free tilted pulses

Szatmari *et al.* [24] demonstrated that the diffracted pulse from a diffraction grating can propagate without GVD temporal spreading in a dispersive medium beyond the grating if its period d is properly chosen [24]. In Fig. 7(a), the experimental setup of Ref. [24] is sketched. The incidence angle β of the incoming plane pulse is chosen so that the diffraction direction for the carrier frequency is perpendicular to the grating. From the angular dispersion curve $\sin\theta(\omega) = K/k(\omega) + \sin\beta/n(\omega)$ produced by the grating, condition $\theta_0 = 0$, and Eqs. (8) and (11), we obtain the angles $\tan\delta = -K/k_0'\omega_0$ and $\gamma = 0°$. The wave fronts and energy of the diffracted pulse propagate along the z direction, with a tilted pulse front due to the grating-induced angular dispersion [see Fig. 7(a)]. For arbitrary grating constant K, the GVD vector does not vanish, but points always in the z direction, its magnitude being, from Eq. (15), $k''_{0,z} = k''_0 - K^2/k_0\omega_0^2$. Consequently, pulse duration grows only with increasing distances from the grating

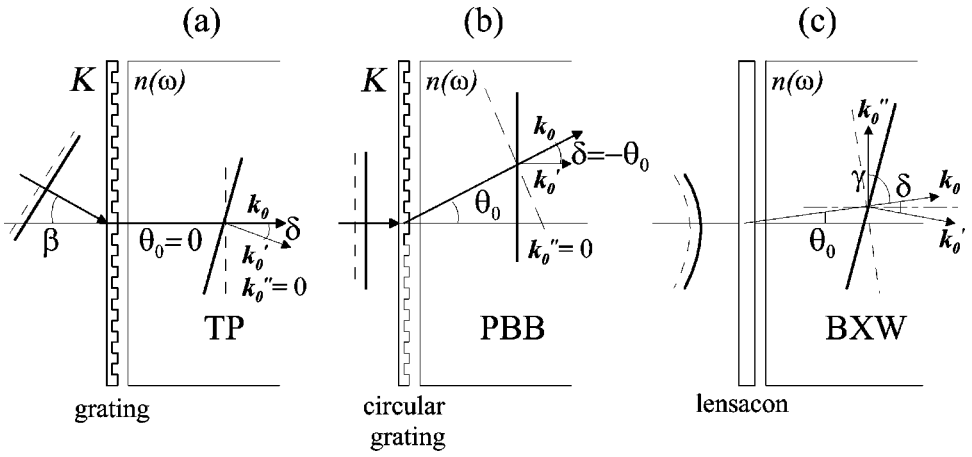

FIG. 7. Three previously reported cases of GVD suppression with (a) TPs, (b) PBBs, and (c) BXWs. Solid, dashed, and dot-dashed lines represent, respectively, pulse fronts, wave front, and planes of constant duration. In (a) and (b) the GVD vector $\boldsymbol{k}_0''$ is zero (there is no pulse broadening along any direction); in (c) $\boldsymbol{k}_0''$ is perpendicular to the propagation direction (there is no broadening along the propagation direction).

and, in particular, over the tilted pulse front. If, moreover, the grating constant is chosen to be

$$K^2=\omega_0^2 k_0 k_0'', \tag{34}$$

the GVD vector cancels. Under condition (34), pulse duration is constant on all points of the dispersive material. Condition (34) can be seen to be the same as Szatmari's condition for the grating period [24] $d^2=\lambda_0/n_0(dn_g/d\lambda)_0$, by writing $K=2\pi/d$, $k_0''=-(\lambda_0^2/2\pi c^2)(dn_g/d\lambda)_0$ and $n_g=ck_0'$ in Eq. (34).

B. GVD-free pulsed Bessel beams

In Porras' works [22,25], a plane pulse entering perpendicularly into a circular diffraction grating of appropriate constant K is transformed into a PBB that propagates without temporal spreading in the dispersive medium. Indeed, as shown in the preceding section, a PBB spreads, in general, due to a GVD vector $\boldsymbol{k}_0''$ perpendicular to the grating, whose magnitude is given by Eq. (33). The GVD vector then vanishes for a cone angle $\tan^2\theta_0=k_0k_0''/k_0'^2$ or, on account that $\sin\theta_0=K/k_0$, for a grating constant

$$K^2=\frac{k_0^3k_0''}{k_0'^2+k_0k_0''}, \tag{35}$$

which is the result of Ref. [22]. Figure 7(b) sketches, for comparison with Fig. 7(a), the experimental situation, the vectors $\boldsymbol{k}_0$, $\boldsymbol{k}_0'$, and the cone and tilt angles.

C. GVD-free Bessel X waves

Earlier, Sonajalg *et al.* [5–7] demonstrated experimentally that a lensacon (holographic element equivalent to a lens and an axicon, and characterized by certain focal length f and cone angle Θ) illuminated by a point source can produce a BXW that propagates without temporal spreading in a normally dispersive medium [see Fig. 7(c)]. The required angular dispersion in the BXW is attained by controlling the distances $f+d$ source-lensacon (d defocusing) and l lensacon medium. In their simple model [7], the cone dispersion curve produced by the lensacon

$$\theta(\omega)=\frac{1}{n(\omega)}\frac{\Theta}{1-\frac{d}{f}\frac{l}{f+d}+\left(\frac{\omega}{\omega_0}-1\right)\left(\frac{l}{f+d}+1\right)}, \tag{36}$$

with $n(\omega)=n_0+n_1(\omega/\omega_0-1)$, is introduced into condition $k_{0,z}''=0$ for suppression of broadening along the z axis, to obtain the relation [7]

$$\Theta=\left[\frac{2n_0n_1}{3\left(\frac{l}{f+d}\right)^2+4\frac{l}{f+d}+1+2\frac{d}{f}\frac{l}{f+d}\left(\frac{l}{f+d}+1\right)}\right]^{1/2}\times\left(1-\frac{d}{f}\frac{l}{f+d}\right)^2 \tag{37}$$

among the system parameters $f+d$, l, and Θ. For the experimental values $f=300$ mm, $d=127$ mm, $n_0=1.56$, and $n_1=0.0325$ (for $\omega_0=3.088$ fs^{-1}) [7], Eq. (37) yields $\Theta=0.013$ rad. Then the cone dispersion curve allows us to obtain the angles $\theta_0=1.2°$, $\delta=-7.0°$, and $\gamma=88.8°$. There are therefore significant differences with respect to the Porras case [22]. The vectors $\boldsymbol{k}_0$, $\boldsymbol{k}_0'$, $\boldsymbol{k}_0''$, wave fronts, pulse fronts, and planes of constant duration of the associated TP are sketched in Fig. 7(c) for comparison with Fig. 7(b). The GVD-free wave of Sonajalg *et al.* [7] is then a nondegenerated, two-tailed ($\theta_0+\delta=-5.8\neq 0$) BXW that propagates at subluminal group velocity, with the peculiarity that $\theta_0+\gamma=90°$, that is, the GVD vector $\boldsymbol{k}_0''$ is perpendicular to the z direction.

Summarizing, the common point of GVD-free TPs and PBBs is the complete suppression of the GVD vector, that is, of pulse broadening in any direction, a situation that can be referred to as "strong" GVD suppression. Indeed, GVD-free PBBs without symmetry revolution would be the same as the GVD-free TP, except for the illumination angle. In the case of GVD-free BXW, "weak" GVD suppression is achieved, in the sense that only the component of the GVD vector along the propagation direction is eliminated. This economy makes BXWs more flexible for GVD suppression in different situations, as we shall see in the following section.

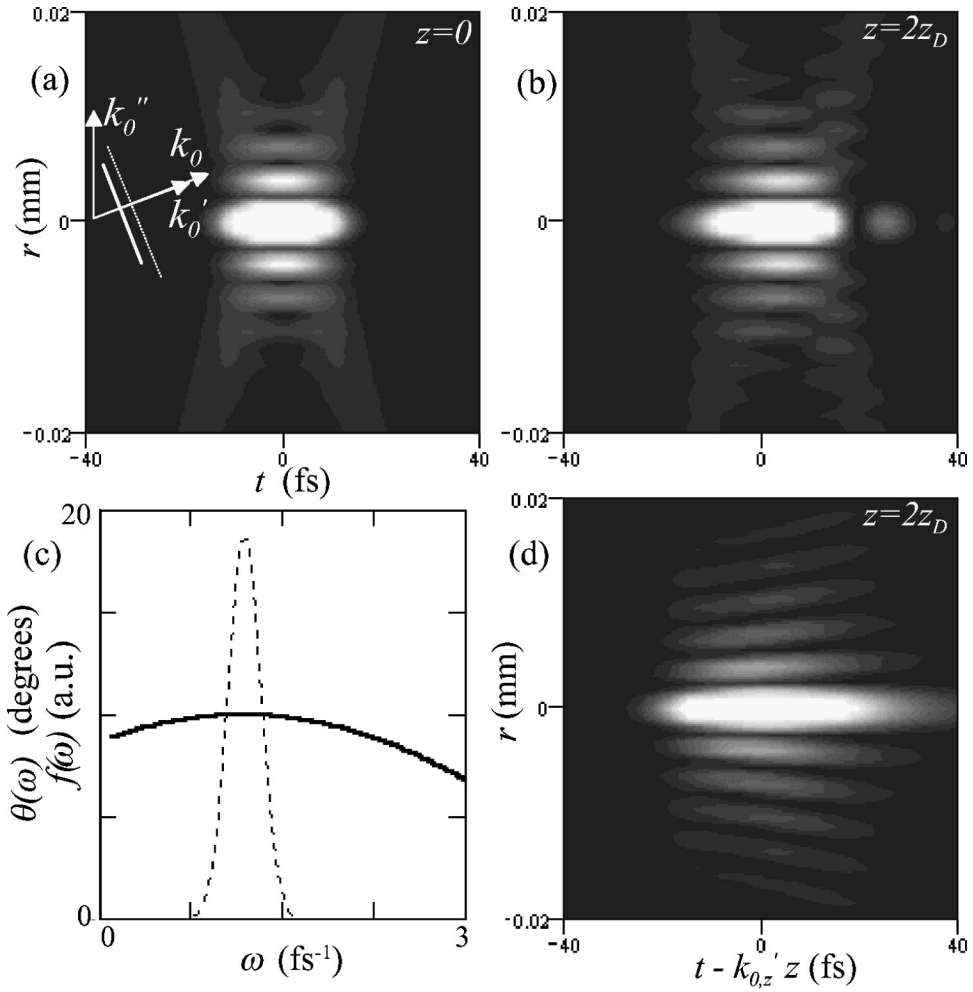

FIG. 8. Inset: schematic drawing of the vectors $\boldsymbol{k}_0$, $\boldsymbol{k}_0'$, and $\boldsymbol{k}_0''$ of the TP associated to the GVD-free BXW in anomalous dispersive media. (a,b): Gray scale plots of the intensity $|E(\boldsymbol{r},t)|^2$ of a GVD-free BXW propagating in fused silica. The carrier frequency $\omega_0 = 1.177\ \mathrm{fs}^{-1}$ is in the anomalous dispersion spectral region of fused silica ($k_0 = 5668\ \mathrm{mm}^{-1}, k_0' = 4880\ \mathrm{fs/mm}, k_0'' = -34.07\ \mathrm{fs}^2/\mathrm{mm}$). The initial on-axis pulse duration is $\Delta t = 10.68$, and the propagation distances are $z = 0$ and $z = 2z_D$, with $z_D = 1.643$ mm. (c): Angular dispersion curve (solid curve) $\theta(\omega) = \theta_0 + \theta_0''(\omega - \omega_0)^2/2$ of the GVD-free BXW, with $\theta_0 = 10°$ and θ_0'' given by Eq. (38), and spectral amplitude (dashed curve) $\hat{f}(\omega) \propto \exp[-\Delta t^2(\omega - \omega_0)^2/4]$. (d) BXW of the same frequency and initial duration, but without angular dispersion [$\theta(\omega) = \theta_0$], after the same propagation distance $z = 2z_D$ in the same medium.

V. GVD SUPPRESSION IN ANOMALOUS DISPERSIVE MEDIA WITH BESSEL X WAVES

As angular dispersion in TPs always creates anomalous GVD [19] [see also Eq. (15)], it is generally believed that angular dispersion can only compensate for normal material dispersion ($k_0'' > 0$). Note also that the negative sign of angular GVD in TPs is independent of the sign of θ_0' (i.e., of making bluer spectral components to propagate at larger angles or vice versa, as pointed out in Ref. [19]). This belief has been reinforced by the fact that the cone dispersion of PBBs, and in the BXWs of Sonajalg *et al.*, can only cancel normal material dispersion [Eqs. (35) and (37) with $k_0'' < 0$ yield imaginary values for the grating constant or the axicon angle]. In this section, we show that there still exist BXWs that can propagate without GVD temporal spreading in a medium with anomalous dispersion.

Indeed, BXWs with cone dispersion of the form $\theta(\omega) \simeq \theta_0 + \theta_0''(\omega - \omega_0)^2/2$, $\theta_0'' < 0°$, i.e., with a maximum $\theta_0 > 0°$ at ω_0, propagate in vacuum with a positive GVD given, from Eq. (22), by $k_{0,z}'' = -(\omega_0/c)\theta_0'' \sin\theta_0 > 0$. In a medium with anomalous dispersion ($k_0'' < 0$), the effective GVD $k_{0,z}''$ can then be made equal to zero if θ_0'' takes, according to Eq. (22), the value

$$\theta_0'' = \frac{k_0''}{k_0} \frac{1}{\tan\theta_0}. \tag{38}$$

We then see that for each carrier frequency ω_0 for which material dispersion is anomalous, there is a family of BXWs, with the cone angle as a free parameter, that propagate without GVD temporal spreading. For all of them, the tilt angle, from Eq. (8) $\delta = 0°$, and the GVD angle, from Eq. (11), are such that $\gamma + \theta_0 = \pi/2$ (weak GVD suppression). The vectors $\boldsymbol{k}_0$, $\boldsymbol{k}_0'$, and $\boldsymbol{k}_0''$, wave fronts, pulse front, and planes of con-

stant width of the associated TP are shown in the inset of Fig. 8(a) [note the peculiarity that this TP is actually nontilted ($\delta=0$) and spreads due to a negative GVD $k''_{0,u_0}=k''_0<0$ along its propagation direction $\boldsymbol{k}_0$]. The BXWs of this family differ in their effective phase and group velocities, $v_{p,z}=\omega_0/k_0\cos\theta_0$, $v_{g,z}=1/k'_0\cos\theta_0$, the radius of the core of Bessel behavior $r_B=\Delta t/k'_0\sin\theta_0$ and its Bessel spot size $\Delta r_B=2.4/k_0\sin\theta_0$, both independent of z and time, and the inclination of the tails, θ_0.

The expected GVD-free behavior of BXWs in anomalously dispersive media is confirmed by numerical simulation [Figs. 8(a) and 8(b)] of a BXW propagating in fused silica, with carrier frequency $\omega_0=1.177$ fs^{-1} in the anomalous dispersion spectral region ($k_0=5668$ mm^{-1}, $k'_0=4880$ fs/mm, $k''_0=-34.07$ fs^2/mm), with angular dispersion curve [Fig. 8(c), solid curve] $\theta(\omega)=\theta_0+\theta''_0(\omega-\omega_0)^2/2$, $\theta_0=10°$, and with θ''_0 given by Eq. (38). We see that at distances larger than the dispersion length $z_D=\Delta t^2/2|k''_0|$ [Fig. 8(b)], or distance at which a plane pulse would broaden by a factor of 2, the duration of the BXW is essentially the same as at $z=0$ [Fig. 8(a)]. Small pulse distortion observed at $2z_D$ originates from third and higher-order dispersion. For comparison, Fig. 8(d) shows a BXW without angular dispersion (all frequencies with same cone angle θ_0) at the same propagation distance in the same medium.

VI. CONCLUSIONS

We have studied diffraction-free BXWs with cone dispersion propagating either in free space or in homogeneous, isotropic, dispersive media. It is not necessary to perform integral in Eq. (17), defining BXWs to describe their propagation features (indeed, this is not generally possible), since they can be predicted from those of the associated, two-dimensional TP having the same angular dispersion curve $\theta(\omega)$.

The spatiotemporal behavior of a TP is determined, up to the second order in dispersion, by the vectors $\boldsymbol{k}_0$, $\boldsymbol{k}'_0$, and $\boldsymbol{k}''_0$, whose moduli and directions can be straightforwardly obtained from the angular dispersion curve and the material constants. The $\boldsymbol{k}_0^{(i)}$ vectors generalize the scalar quantities $k_0^{(i)}$ to describe the joint effects of material and angular dispersion on pulse propagation.

The temporal characteristics of TPs and BXWs with cone dispersion, such as the phase, group velocities, and effective GVD, differ only because of the different angles formed by the vectors $\boldsymbol{k}_0$, $\boldsymbol{k}'_0$, and $\boldsymbol{k}''_0$ with their corresponding privileged spatial directions—the energy flow direction ($\boldsymbol{k}_0$) for TPs and the revolution axis (z) for BXWs. These angles are, respectively, 0°, δ (tilt angle), and γ (GVD angle) for TPs, and θ_0 (cone angle), $\theta_0+\delta$, and $\theta_0+\gamma$ for BXWs. The Bessel-shaped and X-shaped structures of dispersive BXWs, and their modifications during propagation, also reflect those of TPs, as described by the $\boldsymbol{k}_0^{(i)}$ vectors. Let us mention that the described features of TPs and BXWs with cone dispersion are not limited to the particular Gaussian spectrum used in most of the numerical simulations, but are expected to be similar for other spectra of comparable bandwidth, as one can intuitively expect from the physical picture of pulse shape formation.

From our unified approach, we could also describe PBBs as a degenerated class of BXWs, and understand the similarities and differences between the three previously reported cases of GVD suppression in normally dispersive materials with TPs, PBBs, and BXWs. We have predicted, finally, the possibility of using BXWs with cone dispersion (but not TPs or PBB) to achieve GVD-free pulse transmission in media with anomalous dispersion.

ACKNOWLEDGMENTS

The authors acknowledge financial support from MIUR under Project Nos. COFIN 01 and FIRB 01.

[1] J. Durnin, J.J. Miceli, Jr., and J.H. Eberly, Phys. Rev. Lett. **58**, 1499 (1987).
[2] J. Lu and J.F. Greenleaf, IEEE Trans. Ultrason. Ferroelectr. Freq. Control **37**, 438 (1990).
[3] P. Saari and K. Reivelt, Phys. Rev. Lett. **79**, 4135 (1997).
[4] J. Salo, J. Fagerholm, A.T. Friberg, and M.M. Salomaa, Phys. Rev. E **62**, 4261 (2000).
[5] P. Saari and H. Sonajalg, Laser Phys. **7**, 32 (1997).
[6] H. Sonajalg and P. Saari, Opt. Lett. **21**, 1162 (1996).
[7] H. Sonajalg, M. Ratsep, and P. Saari, Opt. Lett. **22**, 310 (1997).
[8] G. Valiulis, J. Kilius, O. Jedrkiewicz, A. Bramati, S. Minardi, C. Conti, S. Trillo, A. Piskarskas, and P. Di Trapani, OSA Trends Opt. Photonics Ser. **57**, 1 (2001).
[9] P. Di Trapani, G. Valulis, A. Piskarskas, O. Jedrkiewicz, J. Trull, C. Conti, and S. Trillo, e-print physics/0303083v1.
[10] C. Conti, S. Trillo, P. Di Trapani, G. Valiulis, O. Jedrkiewicz, and J. Trull, Phys. Rev. Lett. **90**, 170406 (2003).
[11] S. Trillo, C. Conti, P. Di Trapani, O. Jedrkiewicz, J. Trull, G. Valiulis, and G. Bellanca, Opt. Lett. **27**, 1451 (2002).
[12] S. Orlov, A. Piskarskas, and A. Stabinis, Opt. Lett. **27**, 2103 (2002).
[13] O.E. Martinez, Opt. Commun. **59**, 229 (1986).
[14] P. Di Trapani, D. Carioni, G. Valiulis, A. Dubietis, R. Danielius, and A. Piskarskas, Phys. Rev. Lett. **81**, 570 (1998).
[15] X. Liu, L.J. Qian, and F.W. Wise, Phys. Rev. Lett. **82**, 4631 (1999).
[16] M. Topp and G.C. Orner, Opt. Commun. **13**, 276 (1975).
[17] Zs. Bor and B. Racz, Opt. Commun. **54**, 165 (1985).
[18] Zs. Bor, B. Racz, G. Szabo, M. Hilbert, and H.A. Hazim, Opt. Eng. **32**, 2501 (1993).
[19] O.E. Martinez, J.P. Gordon, and R.L. Fork, J. Opt. Soc. Am. A **1**, 1003 (1984).
[20] O.E. Martinez, J. Opt. Soc. Am. B **3**, 929 (1986).
[21] E.B. Treacy, IEEE J. Quantum Electron **QE-5**, 454 (1969).
[22] M.A. Porras, Opt. Lett. **26**, 1364 (2001).
[23] M.A. Porras, Phys. Rev. E **65**, 026606 (2002).

[24] S. Szatmari, P. Simon, and M. Feuerhake, Opt. Lett. **21**, 1156 (1996).
[25] M.A. Porras, R. Borghi, and M. Santarsiero, Opt. Commun. **206**, 235 (2002).
[26] M. Born and E. Wolf, *Principles of Optics*, 7th ed. (Cambridge University Press, Cambridge, 1999).
[27] G.P. Agrawal, *Nonlinear Fiber Optics* (Academic Press, San Diego, 1995).
[28] L. Niggl, T. Lanzl, and M. Maier, J. Opt. Soc. Am. A **14**, 27 (1997).